IEEE Access
Multidisciplinary | Rapid Review | Open Access Journal

Received April 28, 2020, accepted May 11, 2020, date of publication May 18, 2020, date of current version June 2, 2020.

Digital Object Identifier 10.1109/ACCESS.2020.2995293

Multi-Objective Genetic Algorithm Based Coordinated Second- and Third-Order Harmonic Voltage Injection in Modular Multilevel Converter

LEI LIN, (Member, IEEE), ANG LI, CHEN XU, (Member, IEEE), AND YIFAN WANG
State Key Laboratory of Advanced Electromagnetic Engineering and Technology, School of Electrical and Electronic Engineering, Huazhong University of Science and Technology, Wuhan 430074, China

Corresponding author: Chen Xu (xuchen_hust@sina.com)

This work was a part of the projects, Research on Optimal Operation and Control Strategy for Full-Bridge Sub-Modules Involved Modular Multilevel Converters (51677077) and Research on Loss Optimization and Capacitance Reduction of Capacitor-Switching Semi-Full-Bridge (SC-SFB) MMC Sub-Module Based on SiC-MOSFETs and Si-IGBTs (51807073), both sponsored by National Natural Science Foundation of China.

ABSTRACT The submodule (SM) capacitor voltage ripple and the root mean square (RMS) of the arm current are related to the costs and losses of the modular multilevel converter (MMC). The optimization issues have received great attention. The second-order circulating current control and third-order harmonic voltage injection are two conventional optimization methods, but the existing research neglects their coupling effects. In this paper, these two methods are comprehensively investigated and coordinately combined. First, the various performances of MMC under multiple injections are characterized. Then, a multi-objective optimization model considering the output capability of arm voltage and the energy balance of capacitors, is proposed to reduce the SM capacitor voltage ripple and the RMS of the arm current. The amplitudes and phases of the injected second- and third-order harmonic voltages are designed coordinately by genetic algorithm. The simulation and experimental results have validated the effectiveness and feasibility of the proposed method.

INDEX TERMS Modular multilevel converter, third-order harmonic voltage injection, circulating current control, multi-objective optimization, genetic algorithm.

I. INTRODUCTION

Modular multilevel converter (MMC) is extensively discussed owing to the advantages of high modularity, low switching frequency, low output harmonics and high capacity scalability. It has become a mainstay for voltage source converter based high voltage direct current (VSC-HVDC) transmission, especially in long distance transmission, asynchronous power grid interconnection and multi-terminal grid applications [1]–[4]. Currently, the important optimal objectives for MMC are to reduce the costs and losses [5], [6]. The submodule (SM) capacitor accounts for almost half of the SM volume and weight, and one third of the cost. The capacitor voltage ripple suppression can reduce the requirement for the capacitance. In addition, the power losses are mainly related to the switch current or the arm current. The limitation of the arm root-mean-square (RMS) current can reduce the power losses directly.

The associate editor coordinating the review of this manuscript and approving it for publication was Yonghao Gui.

The second-order harmonic circulating current is an inherent problem in regular MMC operation, which has been considered to increase the current stresses and power losses. Much of the conventional research presents the suppression control strategies by injecting controlled second-order harmonic voltage [7]–[9]. Moreover, the circulating current has a significant impact on the capacitor voltage ripples, and the capacitor voltage ripple suppression can be realized by an active second-order harmonic injection [10]. An optimization algorithm is proposed to determine the optimal circulating current to reduce the amplitude of the capacitor voltages [11]. The full-bridge SM (FBSM) is capable of negative voltage level outputs, which enables FBSM-MMC and hybrid MMC operate under the over-modulation condition [12]. For half-bridge SM (HBSM) MMC, third-order harmonic voltage injection also have the same effect, which is similar to the over-modulation in FBSM/hybrid MMC. Higher frequency harmonic injection method is applied in MMC for motor drive with low-speed/low-frequency operation. However, it is not applicable for MMC in the power grid field with fundamental frequency [13]–[15].

The third-order harmonic voltage injection impact is analyzed [16] and has an effect on reducing the capacitor voltage ripple and the RMS of arm current [17], [18]. An exhaustion method which determines the optimized amplitude and phase of third-order harmonic voltage injection are developed [19]. But the capacitor voltage ripple caused by the second-order harmonic does not decrease. The inclusion of the third-order harmonic voltage in coordination with the circulating current injected to the arm voltage reference is considered [15], [20], [22]. However, the third-order harmonic voltage is fixed without taking the second-order harmonic into consideration, and the RMS of arm current may increase [23]. There is a linear programming optimization approach has been taken to analyze the third-order harmonic injection combined with the second-order circulating current injection method [21].

The second-order harmonic circulating current is regulated by adding the second-order differential voltage to the arm voltage reference. Accordingly, the magnitude and phase of the circulating current are adjusted for various objectives [24]. Both the second- and third-order harmonic voltage would appear in the arm voltage. And the over-modulation range depends on the peak value of the arm voltage. Thus, for further reducing the capacitor voltage ripple and RMS of arm current by multiple injection, it is important to coordinate the injected second- and third-order harmonic voltage. It is necessary to design a multi-objective optimization, which is constrained by the output capability of the arm voltage and the energy balance of capacitors.

Most of the traditional multi-objective optimization algorithms transform the problems into single-objective problems and solve them with the help of mathematical programming tools. The commonly used transformation methods include the weighted method, the specific constraint method [25], [26], the min-max approach [27], [28], etc. These methods require decision makers to provide the weight information and subjectivity, which reduces the accuracy of the optimal solution. The genetic algorithm has the characteristic of global parallel search on the population. The method can search in a large space to obtain the optimal solution [29]. And this approach is adopted for multi-nonlinear constraint problems in this paper. However, limited by control chip, the method is only applied off-line to design the optimal injection and chose the optimal devices.

The rest of this paper is organized as follows. Section II compares different circulating current conditions with different second-order harmonic voltage injections. Section III presents the over-modulation can reduce the capacitor voltage ripple and RMS of arm current, then explains the strong coupling relationship and feasibility of second- and third-order harmonic injection based on the MMC differential and common mode model. In Section IV, the original expressions of the objective function which are constrained by the output capability of the arm voltage and the energy balance of capacitors are presented. In section V, the second- and third-order harmonic injection optimization solution is obtained by the genetic algorithm and verified by simulation. Section VI presents the experimental results. Section VII provides the discussion of application and limitation and Section VIII concludes the whole paper.

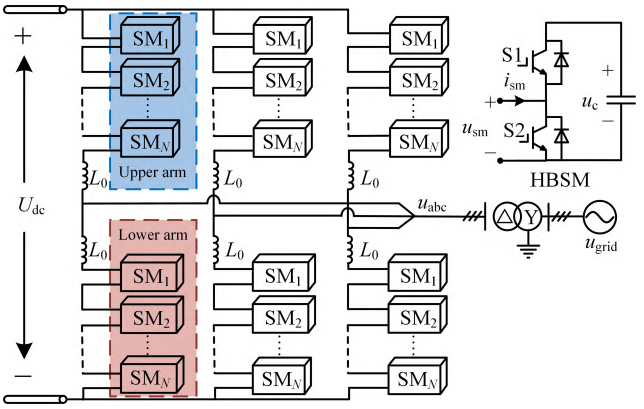

FIGURE 1. Configuration of three-phase MMC.

II. CIRCULATING CURRENT CONTROL FOR MMC

Three-phase MMC which comprises six identical arms is depicted in Fig. 1. Each arm consists of N cascaded HBSM connected with an arm buffer inductor.

To analyze a more general situation, certain assumptions must be made. The analysis in this paper is based on symmetric operation [16]. Thus, second-order harmonic current is considered the major ac component in the circulating current. The upper and lower arm currents i_p and i_n can be expressed as

$$i_p = \frac{I_{dc}}{3} + \frac{I_m}{2}\sin(\omega t + \varphi) + I_{2m}\sin(2\omega t + \gamma) \quad (1)$$

$$i_n = \frac{I_{dc}}{3} - \frac{I_m}{2}\sin(\omega t + \varphi) + I_{2m}\sin(2\omega t + \gamma) \quad (2)$$

where I_{2m} and γ are the amplitude and phase angle of the second-order harmonic circulating current, respectively. φ is the power factor angle. I_m is the amplitude of the fundamental ac-side output current of MMC. I_{dc} is the dc-link current. Because of the symmetry of the three phases, I_{dc} would be divided into three equal parts, and it constitutes the dc component of the circulating current.

Thus, the upper and lower arm reference voltages u_p and u_n can be expressed as

$$u_p = \frac{U_{dc}}{2} - U_m \sin\omega t \quad (3)$$

$$u_n = \frac{U_{dc}}{2} + U_m \sin\omega t \quad (4)$$

where U_{dc} and U_m represent rated dc-link voltage and the amplitude of the ac output voltage, respectively.

The modulation index m is defined as

$$m = \frac{2U_m}{U_{dc}} \quad (5)$$

The second-order harmonic circulating current can be controlled by the closed-loop controller. The performance of

MMC can be improved by different second-order harmonic circulating current control schemes.

A. NATURAL CIRCULATING CURRENT

The circulating current is generated because of the phase common-mode voltage oscillation. From [15], disregarding the injected second order harmonic common-mode voltage in the arm reference voltage, the natural internal circulating current i_{cir} is

$$i_{cir} = \frac{I_{dc}}{3} + \frac{P}{3}\left(\frac{1}{8\omega^2 CL_0U_c - U_{dc}}\right)\cos(2\omega t + \varphi) \quad (6)$$

where P is the active power. L_0 is the arm inductance. C is the SM capacitor. U_c is the rated SM capacitor voltage.

When MMC is in normal operation, the power losses of SMs are less than 1% of the rated power [30]. Ignoring the losses, the active power should achieve balance between the input and the output for MMC, which is given by

$$P = \frac{3}{2}I_m U_m \cos\varphi = I_{dc}U_{dc} \quad (7)$$

Generally, the RMS of the arm current is considered to basically reflect the power losses of MMC. The RMS of the arm current I_r with second order harmonic circulating current can be expressed as

$$I_r = \sqrt{\left(\frac{I_{dc}}{3}\right)^2 + \left(\frac{I_m}{2\sqrt{2}}\right)^2 + \left(\frac{I_{2m}}{\sqrt{2}}\right)^2} \quad (8)$$

Substituting (6) and (7) into (8), the natural RMS of arm current without circulating current control is

$$I_r = \frac{I_{dc}}{3}\sqrt{1 + \frac{2}{m^2\cos^2\varphi} + \frac{1}{2\left(8\omega^2 CL_0/N - 1\right)^2}} \quad (9)$$

B. SUPPRESSED CIRCULATING CURRENT

For power loss reduction of semiconductor devices, the second-order harmonic circulating current is completely suppressed. Thus, the RMS of the arm current is minimized and only the dc-component exists in circulating current. When the I_{2m} is set to zero, the circulating current becomes

$$i_{cir} = \frac{I_{dc}}{3} \quad (10)$$

The minimized RMS of arm current can be obtained as

$$I_r = \frac{I_{dc}}{3}\sqrt{1 + \frac{2}{m^2\cos^2\varphi}} \quad (11)$$

Hence, the power losses of semiconductor devices decrease by completely eliminating second-order harmonic circulating current.

C. INJECTED CIRCULATING CURRENT

Because the arm inductors are small, and the voltage drop and energy in the inductors can be ignored [15]. The upper and lower arm powers p_p and p_n can be expressed as

$$p_p = i_p u_p \quad (12)$$

$$p_n = i_n u_n \quad (13)$$

Power oscillations are equal to the sum of the SM capacitors energy fluctuations, which can be described as

$$\int p_{p(n)}dt = 2NCU_c^2\varepsilon = 2NCU_c\widetilde{u}_{cp(n)} \quad (14)$$

where ε stands for the capacitor voltage ripple rate. Then capacitor voltage ripple can be represented as [20]

$$\begin{aligned}\widetilde{u}_{cp(n)} &= \pm\left[\frac{mI_{dc}}{6\omega C}\cos\omega t - \frac{mI_{2m}}{4\omega C}\sin(\omega t+\gamma) - \frac{I_m}{4\omega C}\cos(\omega t+\varphi)\right] \\ &\quad + \frac{mI_m}{16\omega C}\sin(2\omega t+\varphi) - \frac{I_{2m}}{4\omega C}\cos(2\omega t+\gamma) \\ &\quad \pm \frac{mI_{2m}}{12\omega C}\sin(3\omega t+\gamma)\end{aligned} \quad (15)$$

Thus, injecting second-order harmonic voltage and the resulting second-order harmonic circulating current can be helpful to the SM capacitor voltage ripples. From [14], in order to eliminate the effects of second-order harmonic voltage in arm reference voltage, the optimal circulating current for capacitor voltage ripples reduction is

$$i_{cir} = \frac{I_{dc}}{3} - \frac{mI_m}{4}\cos(2\omega t + \varphi) \quad (16)$$

The additional second-order circulating current injection results in increased arm RMS current compared to suppressed circulating current case in Part A. The corresponding RMS current can be expressed as

$$I_r = \frac{I_{dc}}{3}\sqrt{1 + \frac{2}{m^2\cos^2\varphi} + \frac{1}{2\cos^2\varphi}} \quad (17)$$

Based on the above analysis, the characteristics of the RMS of arm current rate and the capacitor voltage ripple rate are depicted in Fig. 2, with various modulation indexes and power factor angles. It shows that, regardless of the phase angle, the capacitor voltage ripple reduces with the

modulation index increases. And, the method of injecting circulating current is better than the other two cases in reducing the capacitor voltage ripple at the cost of a

relatively small ascension of the RMS of arm current rate. It is an optimal scheme for MMC performance improvement.

III. MULTIPLE VOLTAGE INJECTION FOR MMC

From (7) and (8), it concludes that under constant power transmission, the arm RMS current reduces as the modulation index increases. Regardless of which circulating current control is adopted, the maximized modulation index should be realized for diminishing converter losses.

For the injected circulating current condition, the characteristics of the arm RMS current and capacitor voltage ripple under over-modulation are plotted, shown in Fig. 3. From Fig. 3(a), the arm RMS current has a monotonic decrease with modulation index regardless of the phase angle. From Fig. 3(b), the valley values occur in different modulation

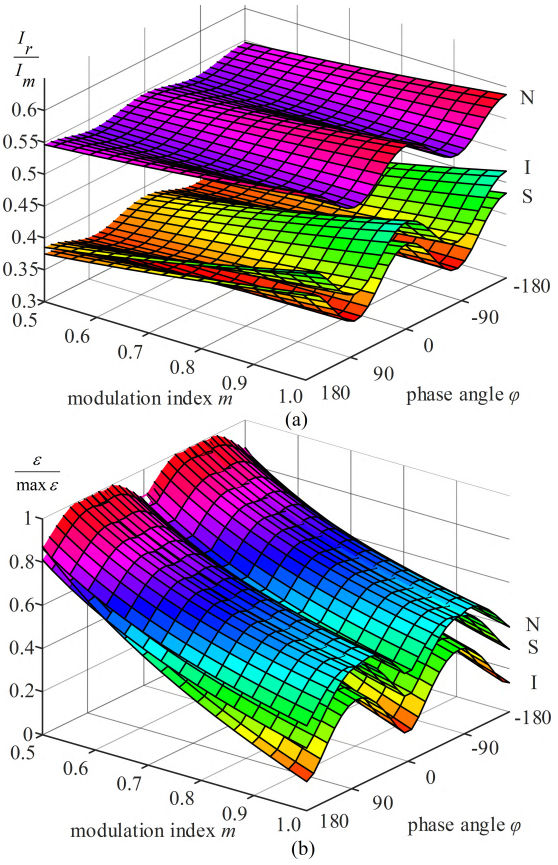

FIGURE 2. Characteristics with various operation condition under different circulating current control. (a) arm RMS current. (b) capacitor voltage ripple.

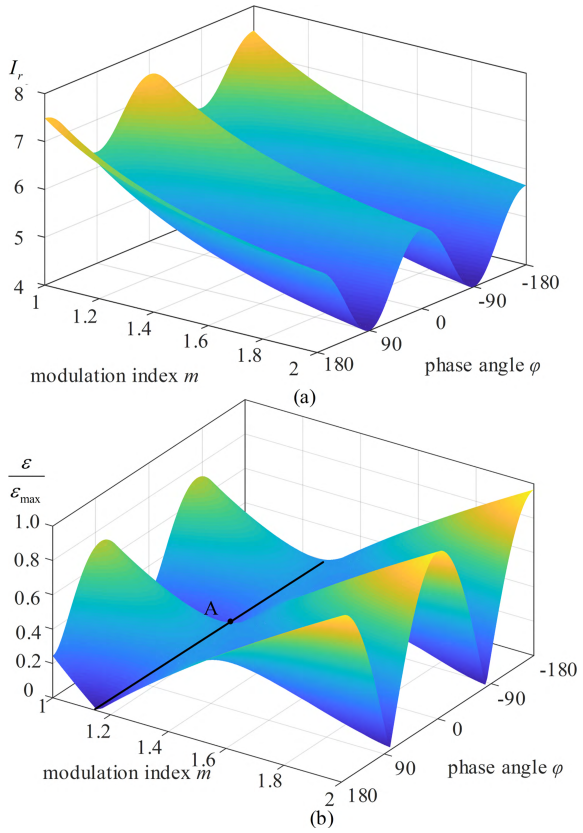

FIGURE 3. Characteristics with over-modulation under injected circulating current control. (a) arm RMS current. (b) capacitor voltage ripple.

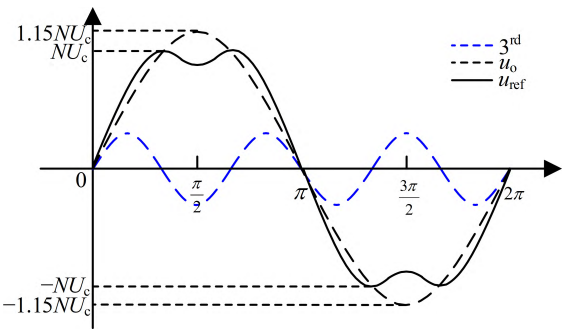

FIGURE 4. Ac components of the arm reference voltage with third-order harmonic voltage injection.

indexes with various phase angles. Taking the unity power factor as an example in the rest of the paper, other operating conditions can be deduced in the same way. When $m = 1.15$, the capacitor voltage ripple rate reaches a minimum. For HBSM-MMC, m is unable to increase the ac output voltage by more than 1.15 times. Third-order harmonic voltage injection is the only way to expand the

modulation index. Thus $m = 1.15$ is considered the optimum point in this case. As widely demonstrated in the existing literature, utilizing the third-order harmonic voltage injection can theoretically expand the modulation index up to 1.15.

As shown in Fig. 4, a schematic diagram of the ac components of the arm reference voltage is depicted. When the magnitude of the three-order harmonic voltage is over 0.167 p.u., the phase angle is determined to be the same as the power factor angle. The ideal fixed third-order harmonic voltage injection makes the ac output voltage to achieve a maximum of $1.15NU_c$.

Note that the other frequency components are generated from the controller modulated dc and fundamental frequency components. Even if the second harmonic is injected in some cases, the purpose is to reduce the second-order harmonic of capacitor voltage ripple. So, these higher harmonics can be ignored in the above analysis [15]. Actually, in Fig. 3(b),

there is a curved surface diagram groove and taking point A when the power factor is 1 as an example. The fundamental frequency and second-order harmonic of the capacitor voltage ripple of point A are suppressed by eliminating the arm power fluctuations of the corresponding frequency components, which can be achieved through coordinating over-modulation and the second-order harmonic circulating injection.

From [31], the voltage and current quantities of MMC are in circular interaction. Fig. 5 depicts the equivalent circuit

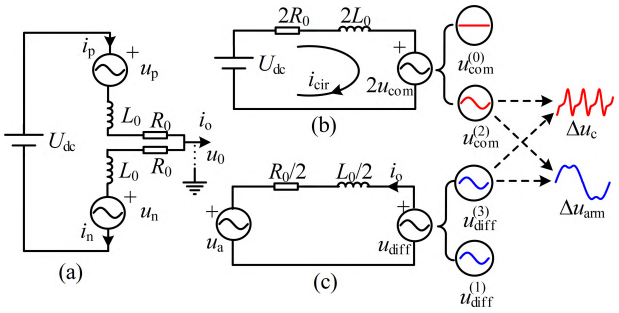

FIGURE 5. MMC equivalent circuits. (a) phase unit. (b) common mode. (c) differential mode.

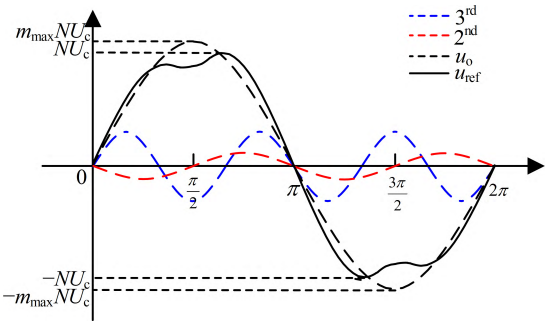

FIGURE 6. Modified ac components of the arm voltage reference with second-order harmonic voltage injection.

of one phase unit, where L_0 and R_0 denote the arm inductance and arm equivalent resistance. The common and differential equivalent circuits are shown in Fig. 5(b) and (c). Fig. 5 reveals that the circulating current is determined by the common mode voltage coexisting on upper and lower arms. The second-order harmonic circulating current influences second-order harmonic SM capacitor voltage variation. And it is coupled with fundamental frequency in switch function, which influences the third-order harmonic voltage. When MMC operate symmetrically, the differential voltage, which is considered to include only fundamental and third-order harmonic voltage here, decides the output current. However, the corresponding third-order harmonic current would disappear in the ac-side current due to the universal Y-Δ connected transformer. So, injecting low frequency harmonics have no effect on the output voltage and current.

In summary, both the second- and third-order harmonic voltage contribute to the transient arm voltage and SM capacitor voltages, and their effects on the arm RMS current and capacitor voltage ripple are strongly coupled. And, it is important that there is no effect on the output current.

Therefore, the arm voltage reference and arm current with second- and third-order harmonic voltage injection are rewritten as

$$u_{p(n)} = \frac{U_{dc}}{2} \mp U_m \sin\omega t \mp v_s U_m \sin 3\omega t \mp v_c U_m \cos 3\omega t + U_{2m}\cos\beta \cdot \sin 2\omega t + U_{2m}\sin\beta \cdot \cos 2\omega t \quad (18)$$

$$i_{p(n)} = \frac{I_{dc}}{3} \pm \frac{I_m}{2}\sin(\omega t + \varphi) + i_s \sin 2\omega t + i_c \cos 2\omega t \quad (19)$$

where variables v_s and v_c are the coefficient of the sine-wave harmonic component and the cosine-wave harmonic component of the third-order harmonic voltage injection, respectively. Variables i_s and i_c represent the sine-wave harmonic component and cosine-wave harmonic component of the second-order circulating current injection, respectively. Both of these variables are decomposed into sine-wave and cosine-wave components, which is beneficial to subsequent derivation. U_{2m} and β denote the corresponding amplitude and phase angle of the second-order harmonic voltage injection, respectively.

Therefore, the arm current can be rewritten as

$$i_{p(n)} = \frac{I_{dc}}{3}\left[1 \pm \frac{2\sin(\omega t + \varphi)}{m\cos\varphi}\right] + i_s \sin 2\omega t + i_c \cos 2\omega t \quad (20)$$

Seeing Fig. 6, the peak value of arm voltage reference changes after considering the injected second-order harmonic voltages. And it decides the range of expanded modulation index. Thus, second- and third-order voltage injection should be arranged in optimal coordination for optimal modulation index.

IV. MMC PERFORMANCE CHARACTERISTIC WITH MULTIPLE INJECTION

Assume that SM losses are neglected and SMs of one arm are not distinguished due to the balancing algorithm combined modulation process [17]. For optimizing performance of MMC, it is necessary to analyze the arm RMS current and capacitor voltage ripples with multiple injection.

A. ANALYSIS OF CAPACITOR VOLTAGE RIPPLE

To address the effects of multiple injection, a detailed capacitor voltage expression should be obtained. The dc-link voltage is built by maintaining the sum output of SMs in the phase leg. For the purpose of developing the analytical formula of instantaneous capacitor voltage, the arm switching functions $S_{p(n)}$ are obtained from [24], given by

$$S_{p(n)} = \frac{1}{2} \mp \frac{1}{2} m \sin\omega t \mp \frac{1}{2} m v_s \sin 3\omega t \mp \frac{1}{2} m v_c \cos 3\omega t \quad (21)$$

For simplicity, the second-order components are neglected in the switching functions, because they have few impacts on the capacitor voltage ripples. Obviously, the SM capacitor current equals to the products of the arm switching function and the arm current. And the capacitor voltage can be expressed as

$$C\frac{du_{cp(n)}}{dt} = S_{p(n)} \cdot i_{p(n)} \quad (22)$$

Subsequently, the capacitor voltage ripples (superscript $\sim$) can be derived as (23) shown at the bottom of the next

page. From (23), the even-order harmonic components of the capacitor voltage ripples in the upper and lower arms are identical. In contrast, odd-order harmonic components of capacitor voltage ripples are out of phase in the upper and lower arms. The modulation index has no effect on the even-order harmonic components but affects the fundamental frequency and third-order harmonic components. On the other hand, the introduced second- and third-order harmonic voltages complicates the capacitor voltage ripples expression. It is necessary to consider the higher harmonic components in the capacitor voltage fluctuation.

B. MODIFIED ARM REFERENCE VOLTAGE

From Fig. 5, the total common mode voltage is formed by the sum of the SMs capacitor voltage output through a phase leg. The common mode voltage is derived as (24). Considering the characteristics of the arm inductor, the relationship between the second-order harmonic voltage and second-order circulating current is expressed as (25).

$$\begin{aligned} 2u_{\mathrm{com}} = {} & NS_{\mathrm{p}}\left(U_{\mathrm{cref}} + \widetilde{u}_{\mathrm{cp}}\right) + NS_{\mathrm{n}}\left(U_{\mathrm{cref}} + \widetilde{u}_{\mathrm{cn}}\right) \\ & + 2U_{2\mathrm{m}}\cos\beta \cdot \sin 2\omega t + 2U_{2\mathrm{m}}\sin\beta \cdot \cos 2\omega t \end{aligned} \tag{24}$$

$$\widetilde{u}^{(2)}_{\mathrm{com}} = -L_0 \frac{\mathrm{d}(i_{\mathrm{s}}\sin 2\omega t + i_{\mathrm{c}}\cos 2\omega t)}{\mathrm{d}t} \tag{25}$$

where u_{com} is the common mode voltage and superscript $\sim$ expresses its ripple. Substituting (25) into (24), the second harmonic voltage can be solved as (26). Therefore, the detailed mathematical expressions of capacitor voltage and modified arm voltage reference are established. The effects of multiple injection on these parameters are obtained.

C. COORDINATED MULTIPLE INJECTION

Based on the above analysis, the expanded modulation index yields increased ac-side output voltage, which enables the converter performance to be improved in two main cases: 1)

$$\begin{aligned} & U_{2\mathrm{m}}\sin\beta \\ & = -2\omega L i_{\mathrm{s}} + \frac{N}{2\omega C}\left(\frac{1}{4}i_{\mathrm{s}} + \frac{1}{6}m^2 i_{\mathrm{s}} + \frac{1}{24}m^2 v_{\mathrm{c}} I_{\mathrm{dc}}\right) \\ & \quad - \frac{N}{2\omega C}\left(\frac{1}{12}v_{\mathrm{c}} I_{\mathrm{dc}} + \frac{1}{8}m^2 v_{\mathrm{c}}^2 i_{\mathrm{s}} + \frac{1}{8}m^2 v_{\mathrm{s}}^2 i_{\mathrm{s}}\right) \end{aligned}$$

$$\begin{aligned} & U_{2\mathrm{m}}\cos\beta \\ & = 2\omega L i_{\mathrm{c}} + \frac{N}{2\omega C}\left(\frac{1}{12}m^2 I_{\mathrm{dc}} + \frac{1}{8}m^2 v_{\mathrm{s}}^2 i_{\mathrm{c}} + \frac{1}{8}m^2 v_{\mathrm{c}}^2 i_{\mathrm{c}}\right) \\ & \quad - \frac{N}{2\omega C}\left(\frac{1}{4}i_{\mathrm{c}} + \frac{1}{4}I_{\mathrm{dc}} + \frac{1}{12}v_{\mathrm{s}} I_{\mathrm{dc}} + \frac{1}{36}m^2 v_{\mathrm{s}} I_{\mathrm{dc}} + \frac{1}{6}m^2 i_{\mathrm{c}}\right) \end{aligned} \tag{26}$$

capacitor voltage ripple reduces under constant power transmission. 2) capacity of MMC has some accordingly increasing margin with the same current stress.

From (8), the capacity increase can be realized by increasing the ac-side output voltage, ac-side output current, dc-link voltage or dc-link current. Limited by the existing manufacturing standard and insulation level, the rated dc-link voltage is generally limited, and it would be constant in practical operation. The expanded modulation index leads to an increased ac-side output voltage. Therefore, the transmission power is promoted with the rest of the variables fixed.

According to (7), the RMS of the arm current and its peak value are bound to increase if the ac-side output current is constant. However, the current rating of the semiconductor device should be considered. A principle is identified that the optimized multiple injection and expanded modulation index would not endanger those semiconductor devices. Thus, the rated arm current needs to be determined to be lower than that before the multiple injection optimization. The capacity ascension margin is no more proportional to that of the expanded modulation index, which is difficult to compare without specific device ratings. Thus, the first case (operating on point A in Fig. 3) is chosen for discussion in this paper.

With the maximal modulation index, the circulating current can be rewritten as

$$I_{\mathrm{r}} = \sqrt{\frac{m^2\cos^2\varphi + 2}{16}I_{\mathrm{m}}^2 + \frac{i_{\mathrm{s}}^2 + i_{\mathrm{c}}^2}{2}} \tag{27}$$

The solution of the optimized multiple injection problem is accessible for constant modulation index expansion and power transmission. The objective functions are obtained as

$$obj.\ \min \begin{cases} \mathrm{g}_1(v_{\mathrm{s}}, v_{\mathrm{c}}, i_{\mathrm{s}}, i_{\mathrm{c}}) = |\widetilde{u}_{\mathrm{c}}| \\ \mathrm{g}_2(i_{\mathrm{s}}, i_{\mathrm{c}}) = i_{\mathrm{r}} \end{cases} \tag{28}$$

$$\begin{aligned} & \widetilde{u}_{\mathrm{cp(n)}} \\ & = \pm\left(\frac{1}{6\omega C}mI_{\mathrm{dc}} - \frac{1}{3\omega C}\frac{I_{\mathrm{dc}}}{m} - \frac{1}{4\omega C}mi_{\mathrm{c}} + \frac{1}{4\omega C}mv_{\mathrm{s}}i_{\mathrm{c}} - \frac{1}{4\omega C}mv_{\mathrm{c}}i_{\mathrm{s}}\right)\cos\omega t \pm \left(-\frac{1}{4\omega C}mi_{\mathrm{s}} - \frac{1}{4\omega C}mv_{\mathrm{s}}i_{\mathrm{s}} - \frac{1}{4\omega C}mv_{\mathrm{c}}i_{\mathrm{c}}\right)\sin\omega t \\ & \quad + \left(-\frac{1}{4\omega C}i_{\mathrm{s}} - \frac{1}{12\omega C}v_{\mathrm{c}}I_{\mathrm{dc}}\right)\cos 2\omega t + \left(\frac{1}{4\omega C}i_{\mathrm{c}} + \frac{1}{12\omega C}I_{\mathrm{dc}} - \frac{1}{12\omega C}v_{\mathrm{s}}I_{\mathrm{dc}}\right)\sin 2\omega t \pm \left(\frac{1}{12\omega C}mi_{\mathrm{c}} + \frac{1}{18\omega C}mv_{\mathrm{s}}I_{\mathrm{dc}}\right)\cos 3\omega t \\ & \quad \pm \left(\frac{1}{12\omega C}mi_{\mathrm{s}} - \frac{1}{18\omega C}mv_{\mathrm{c}}I_{\mathrm{dc}}\right)\sin 3\omega t + \left(\frac{1}{24\omega C}v_{\mathrm{c}}I_{\mathrm{dc}}\right)\cos 4\omega t + \left(\frac{1}{24\omega C}v_{\mathrm{s}}I_{\mathrm{dc}}\right)\sin 4\omega t \\ & \quad \pm \left(+\frac{1}{20\omega C}mv_{\mathrm{s}}i_{\mathrm{c}} + \frac{1}{20\omega C}mv_{\mathrm{c}}i_{\mathrm{s}}\right)\cos 5\omega t \pm \left(\frac{1}{20\omega C}mv_{\mathrm{s}}i_{\mathrm{s}} - \frac{1}{20\omega C}mv_{\mathrm{c}}i_{\mathrm{c}}\right)\sin 5\omega t \end{aligned} \tag{23}$$

TABLE 1. Designed valuables for coordinated multiple.

symbol	*Quantity*	*Min.*	*Max.*
v_s	Sine 3rd voltage	$-30\%U_m$	$30\%U_m$
v_c	Cosine 3rd voltage	$-30\%U_m$	$30\%U_m$
i_s	Sine 2nd circulating current	$-10\%I_m$	$10\%I_m$
i_c	Cosine 2nd circulating current	$-10\%I_m$	$10\%I_m$
m	Modulation index	0	1.15

The objective function is designed for the minimum capacitor voltage ripples and the arm RMS current. The transient capacitor voltage has uncertain valley and peak values, which depends on the injection variables. Since subjects are nonlinear. To find the multiple injection variable solutions under optimal coordination, a nonlinear program problem has been developed. In order to reduce the search area and obtain the optimal solution quickly, the second-order harmonic circulating current amplitude is set to be less than 10% of the fundamental current amplitude. The maximum of the third-order harmonic voltage amplitude is set to be less than 30% of the fundamental voltage amplitude, as shown in Table 1. The limitation above is estimated by calculating a large amount of working conditions. In fact, the constraints can be adjusted according to different conditions. And they can be expanded or removed if not care too much about computational speed.

V. PROPOSED GENETIC ALGORITHM

Based on the above analytical model, the optimization scheme is developed to obtain the optimal multi-objective design. Generally, the efficient solution is not unique, and the set of all efficient solutions is called the Pareto solution. The core of the multi-objective genetic algorithm (MOGA) is to coordinate objective function and find the Pareto solution. By means of the rank of the noninferior solution and the corresponding selection operator, the population moves towards the Pareto solution in the optimization process.

Existing genetic algorithms include vector evaluation-based genetic algorithm, niched Pareto genetic algorithm, and non-dominated sorting genetic algorithm (NSGA), etc. Zitzler and Thiele *et al.* conducted comprehensive analysis and experimental comparison of these methods [32], and the results show that NSGA has the best performance in terms of computational speed and accuracy. NSGA uses a non-dominant classification program to simplify multi-objective to an adaptive function. NSGA-II defines crowding distance to estimate the solution density around a point, instead of fitting value sharing. This algorithm reduces computational complexity and has an optimal retention mechanism. Therefore, NSGA-II will be adopted in this paper [33]. The flowchart of MOGA is presented in Fig. 7.

After input the constant initial parameters of MMC and the variables which are needed to be solved, a fixed-size initial

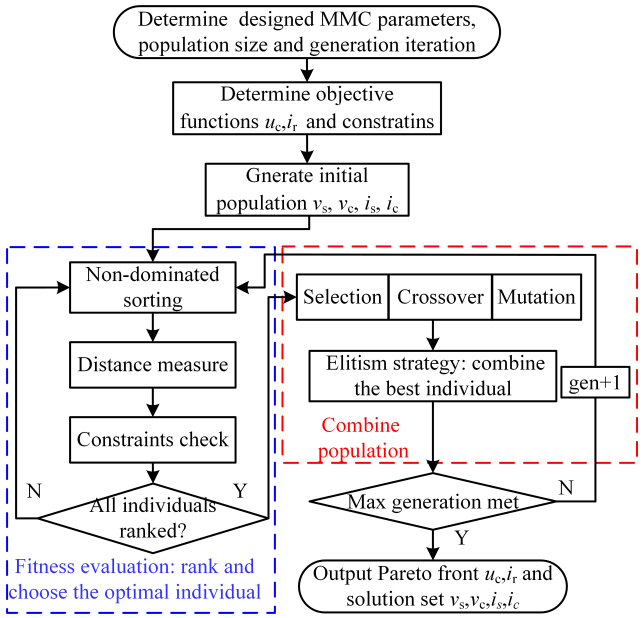

FIGURE 7. Flowchart of MOGA-based multiple injection optimization.

population is randomly generated. Most parameters are set to the default value. For example, the population size set as 50 and generation iteration set as 400. The accuracy is appropriately increased according to whether the calculation can be completed. Each individual in the population consist of variables as solutions. Then the individuals are evaluated by the objective functions and their distance are measured for ranking. Once all individuals are ranked, the Pareto solutions are chosen to be modified by the selection, crossover and mutation. Then, the population is restructured and the generation plus one. The ultimate Pareto solution cannot be obtained until the generation reaches the maximum.

The priority for different objectives should be set in advance to determine the specific solutions under different conditions. In this paper, two parallel objectives are chosen to improve the performance of MMC, namely the minimum capacitor voltage ripple and minimum arm RMS current.

A. CONSTRAINTS

1) OUTPUT CAPABILITY OF ARM VOLTAGE

Because the rated capacitor voltage is a constant, the peak value of the modified arm voltage reference should not exceed the maximum arm voltage value, which is expressed as

$$u_{\text{p(n)-peak}} \leq NU_{\text{cref}} \tag{29}$$

The ultimate optimized peak value of the arm voltage reference is exactly near to the maximum arm output voltage, and it increases the SM capacitor voltage utilization with enhanced MMC performance.

2) ENERGY BALANCE OF CAPACITORS

As indicated from (22), the capacitor current equals to the product of the arm switching function and arm current.

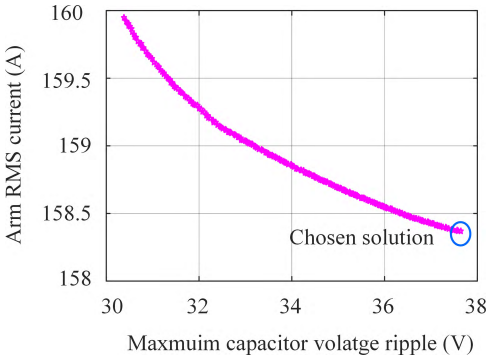

FIGURE 8. Optimization Pareto front with power factor of 1.

To ensure the energy balance in whole fundamental period, the dc capacitor current should equal to zero during the all period, which is restrained as

$$\cos\left(\beta - \arctan\frac{i_c}{i_s}\right) = 0 \tag{30}$$

(30) reveals that the phase angle of the second harmonic voltage is approximately 90° phase leading to the circulating current, which complies with inductor characteristics.

B. SIMULATION RESULT

The solution set obtained by this method is very dense when use MATLAB gamultiobj and gaoptimset function. In this paper, the optimization algorithm is carried out in MATLAB/Global Optimization Toolbox. And this toolbox is a straightforward and convenient method to solve GA problem according to instructions of MATLAB. To validate the effectiveness of the proposed scheme, simulations are constructed using MATLAB/Simulink. Engineering model choose Nanfeng converter station MMC of Shanghai Nanhui wind power plant. The SM capacitance is 6mF. The rated dc-link voltage and the SM number per arm are 60kV and 48, respectively. Thus, the rated capacitor voltage and the ripple is set to be 1250V and 58V.

Fig. 8 shows the Pareto front which gives the multi-objective optimization under given parameters. It shows that the RMS of the arm current and the maximum capacitor voltage ripples are unable to achieve the minimum optimal values simultaneously. In the Pareto front, the capacitor voltage ripple reduces at the cost of promoting the arm RMS current, and vice versa. So, the optimal solution can be acquired according to the actual demands. In this study, the solution corresponds to the lowest arm RMS current is chosen as an example.

The simulation waveforms of the capacitor voltage ripple, arm voltage and arm current are depicted in Fig. 9. Compared with third harmonic injection in [16] and multiple injection without optimization in [19], the peak SM capacitor voltage ripple reduces by 22% and 15% respectively, and the RMS of the arm current decreases by 5.4% and 7.6%. The arm voltage is below NU_c and realize the ideal maximum value 1.15, which is consistent with the above analysis. The simulation results prove the practicability and effectiveness of the proposed method.

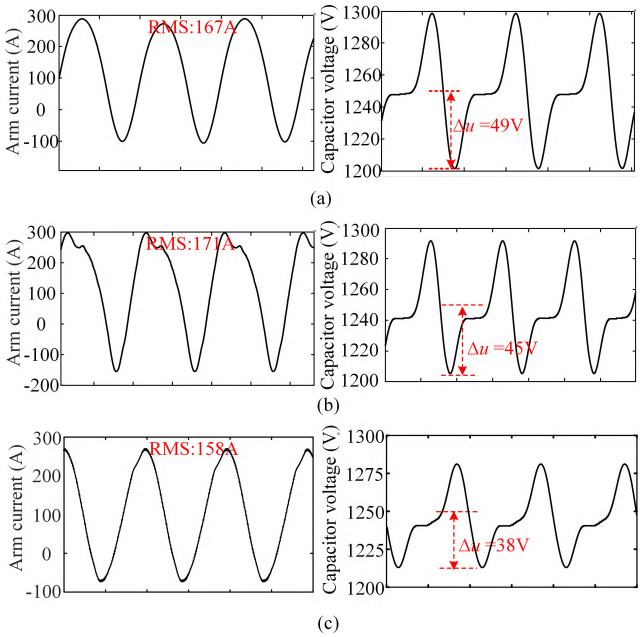

FIGURE 9. Simulation waveforms of the RMS of arm current and capacitor voltage ripple with power factor of 1. (a) third harmonic injection in [17]. (b) multiple injection without optimization in [22]. (c) multiple injection optimization with optimization.

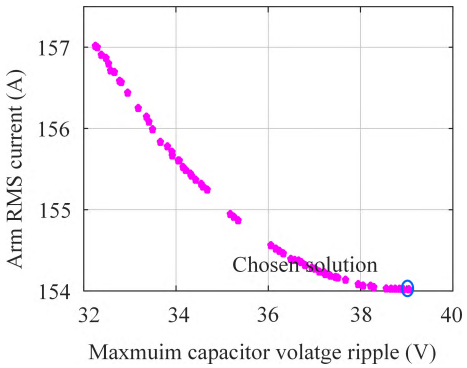

FIGURE 10. Optimization Pareto front with power factor of 0.8.

Fig. 10 shows the Pareto front with power factor of 0.8. The simulation waveforms of the capacitor voltage ripple, arm voltage and arm current are depicted in Fig. 11. Compared with third harmonic injection and multiple injection without optimization, the peak SM capacitor voltage ripple reduces by 25% and 17% respectively, and the RMS of the arm current decreases by 5.5% and 9.4%. From the result, the power factor does not affect the performance of the proposed control method.

In the simulation, the harmonic injection has little effect on the fundamental frequency current control. The second-order harmonic injection method is mainly completed in the circulation suppression controller and the third-order harmonic

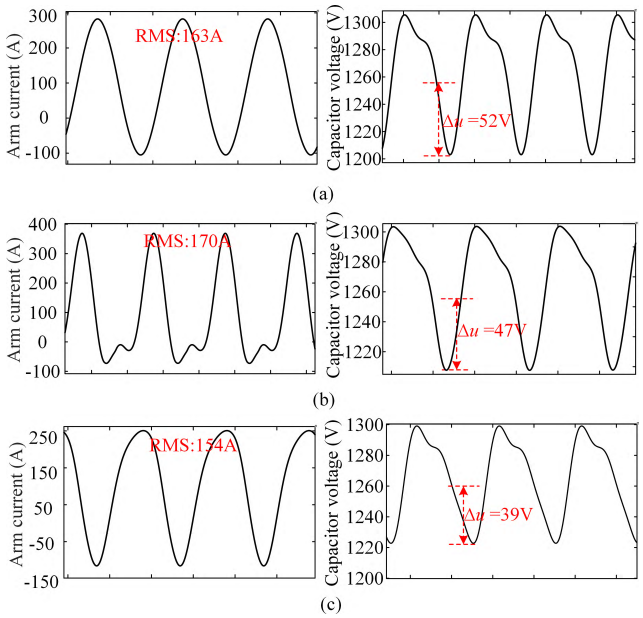

FIGURE 11. Simulation waveforms of the RMS of arm current and capacitor voltage ripple with power factor of 0.8. (a) third harmonic injection in [17]. (b) multiple injection without optimization in [22]. (c) multiple injection optimization with optimization.

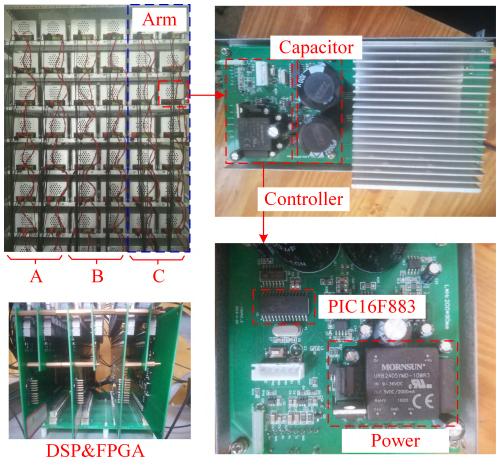

FIGURE 12. Downscaled MMC prototype.

injection method is completed by accumulating the corresponding third harmonics after close-loop control.

VI. EXPERIMENTAL VERIFICATION

A downscaled MMC prototype is built to demonstrate the correctness of the proposed multiple injection scheme. The photograph consisting of six identical arms is shown in Fig. 12. The parameters of the prototype configuration are listed in Table 2. The control system is constructed through a widely-used digital signal processor (DSP) board (TMS320F28335) and three field programmable gate array (FPGA) boards (EP3C25Q240C8N). The DSP generates upper and lower arm reference voltages under closed-loop control. FPGAs implement the modulation process with a capacitor voltage balancing algorithm, then conducts switching signals to SMs by optical fibers. The PIC board (16F883) in each SM receives the switching signals and generates gate drive pulses.

TABLE 2. Experimental parameters.

Parameters	*Symbols*	*A*	*B*
Rated active power	P	1200w	1200w
DC voltage	U_{dc}	160V	160V
AC phase voltage	U_m	80V	92V
AC phase current	I_m	10A	8.7A
SM capacitance	C	3.8mF	3.8mF
Rated capacitor voltage	U_c	40V	40V
Arm SMs number	N	4	4
Modulation index	m	1.0	1.15

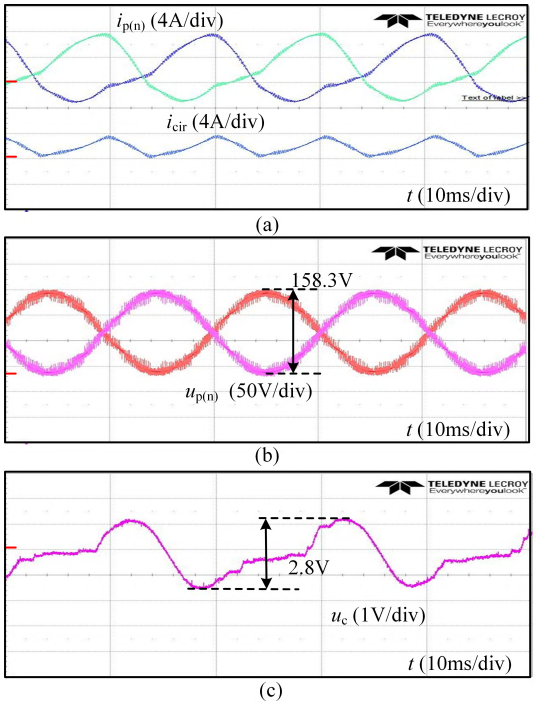

FIGURE 13. Experimental waveforms with natural circulating current. (a) arm and circulating currents. (b) arm voltages. (c) SM capacitor voltage.

A. CIRCULATING CURRENT CONTROL

The experimental results under unity power factor conditions with different circulating control schemes are depicted in Fig. 13-15. The arm voltage contains mainly dc and fundamental frequency components, and the amplitude is approximately 80V due to the limit of dc voltage amplitude in HBSM MMC.

Fig. 13 and Fig. 14 show that the arm circulating currents are composed of dc and second-order harmonic components. With second-order harmonic circulating current suppressed,

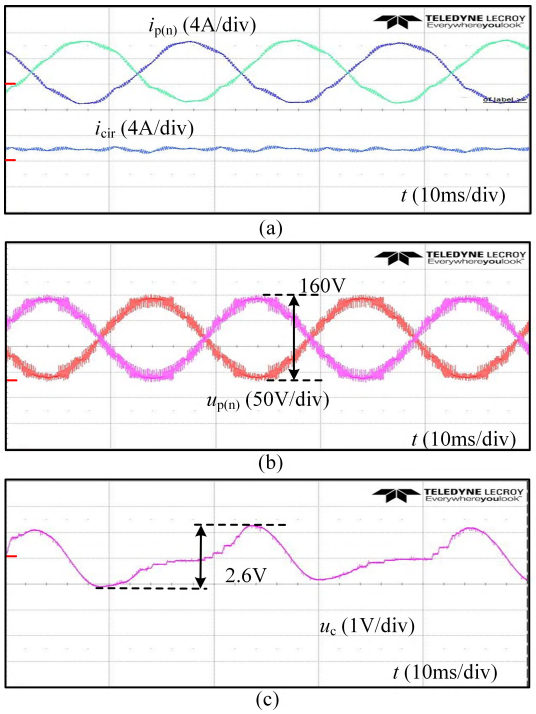

FIGURE 14. Experimental waveforms with suppressed circulating current. (a) arm and circulating currents. (b) arm voltages. (c) SM capacitor voltage.

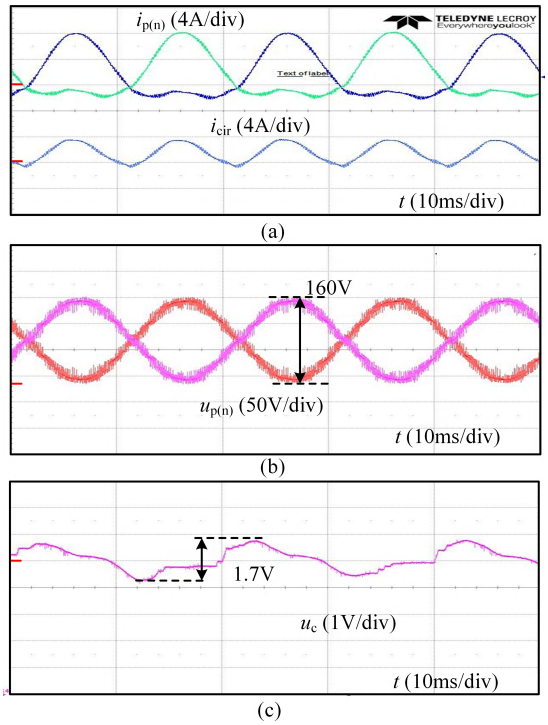

FIGURE 15. Experimental waveforms with injected circulating current. (a) arm and circulating currents. (b) arm voltages. (c) SM capacitor voltage.

both the arm current stress and capacitor voltage ripples reduce. From Fig. 15, the circulating current is actively injected, which causes the arm current to slightly increase

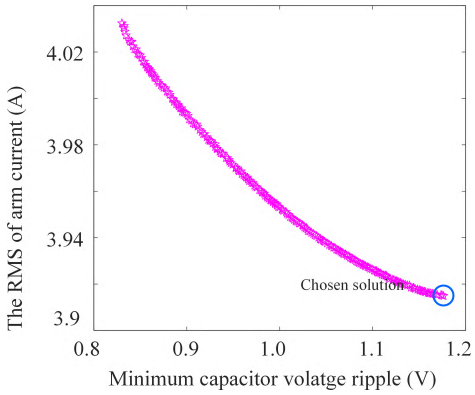

FIGURE 16. Experiment MOGA-based optimization Pareto front.

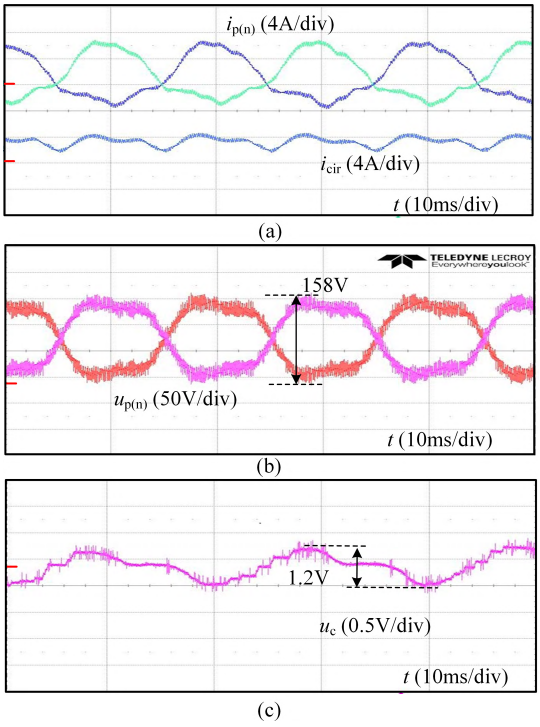

FIGURE 17. Experimental waveforms with coordinated multiple injection. (a) arm and circulating currents. (b) arm voltages. (c) SM capacitor voltage.

from 4.34A to 4.64A. Moreover, compared to the natural circulating current conditions, the SM capacitor voltage ripples are decreased from 2.8V to 1.7V.

B. COORDINATED MULTIPLE INJECTION

The results of the optimization algorithm for experimental conditions are shown in Fig. 16. The solution corresponds to the lowest arm RMS current is still chosen in this section. As shown in Fig. 17, the experimental results with coordinated multiple injection optimization show that arm voltage contains an additional third-order harmonic voltage. Although its amplitude is still approximately 80V, the fundamental component amplitude increases to 92V.

Over-modulation $m = 1.15$ is realized. In addition, with optimal multiple injection, the SM capacitor voltage ripples are further reduced from 1.7V to 1.2V and the RMS of arm current is reduced from 4.64A to 3.94A.

VII. DISSCUSIONS

From [34], [35], the dc-side fault ride-through capability makes FBSM/hybrid MMC becomes a trend in engineering application. However, the method proposed above is limited in HBSM MMC. And there are some differences between FBSM/hybrid and HBSM MMC. So, the method must be further improved if applied in FBSM/hybrid MMC. Challenges are listed as follows. First, the over-modulation operation is not necessarily performed through the third harmonic injection when FBSM exists. Second, it is necessary to re-analyze the coupling between the negative voltage and the injected harmonic voltage. Third, there is a problem of uneven capacitance voltage in hybrid MMC [36].

The capacitor voltage ripples and the RMS of the arm current are part of the factors affecting the costs and losses of MMC. In fact, the costs and losses of MMC are determined by many factors. The method in this paper can analyze more objective functions of influencing factors to further optimize the costs and losses of MMC.

This method adopts the offline optimization mode. There are two application scenarios. First, this method is used to design the optimal capacitor voltage ripple and RMS of the arm current in typical operating condition of the specific engineering. Secondly, an off-line table is generated in the operating conditions. The optimal second- and third-order harmonic injection are chosen by table lookup during online operation. The robustness of the solutions generated by the GA approach is well. The optimal injection will not change abruptly unless the transmission power changes a lot. If applied to the online optimization mode, three problems need to be considered. First, whether the chip can carry the large computation of the algorithm. Second, whether the time of algorithm meets the requirements of the control cycle. Third, how to reasonably select the optimal solution set. These problems require comprehensive consideration of controller selection, multi-objective optimization algorithm selection and online optimization scheme design.

VIII. CONCLUSION

In this paper, the coupling effect of the second- and third-order harmonic injection is considered, which makes fixed injection component not be the optimal method to reduce the capacitor voltage ripple and the RMS of the arm current.

Then, the optimal contents injection is designed to realize the minimum capacitor voltage ripple and the RMS of the arm current with the proposed MOGA, which is constrained to the arm output voltage capability and the energy balance of capacitors. The simulation and experiment verify that the method can reduce the two targets more than the other methods.

Future work will focus on the extension of this method in the FBSM/hybrid MMC and considering the online optimization method.

REFERENCES

[1] A. Lesnicar and R. Marquardt, "An innovative modular multilevel converter topology suitable for a wide power range," in *Proc. IEEE Bologna Power Tech Conf.*, Bologna, Italy, Jun. 2003, pp. 1–6.

[2] A. Nami, J. Liang, F. Dijkhuizen, and G. D. Demetriades, "Modular multilevel converters for HVDC applications: Review on converter cells and functionalities," *IEEE Trans. Power Electron.*, vol. 30, no. 1, pp. 18–36, Jan. 2015.

[3] M. A. Perez, S. Bernet, J. Rodriguez, S. Kouro, and R. Lizana, "Circuit topologies, modeling, control schemes, and applications of modular multilevel converters," *IEEE Trans. Power Electron.*, vol. 30, no. 1, pp. 4–17, Jan. 2015.

[4] C. Xu, Y. Kang, X. Chen, and K. Dai, "Voltage droop control at point of common coupling with arm current and capacitor voltage analysis for distribution static synchronous compensator based on modular multilevel converter," *IET Power Electron.*, vol. 9, no. 8, pp. 1643–1653, Jun. 2016.

[5] H. Akagi, "Classification, terminology, and application of the modular multilevel cascade converter (MMCC)," *IEEE Trans. Power Electron.*, vol. 26, no. 11, pp. 3119–3130, Nov. 2011.

[6] C. Zhao, Y. Li, Z. Li, P. Wang, X. Ma, and Y. Luo, "Optimized design of full-bridge modular multilevel converter with low energy storage requirements for HVdc transmission system," *IEEE Trans. Power Electron.*, vol. 33, no. 1, pp. 97–109, Jan. 2018.

[7] Z. Li, P. Wang, Z. Chu, H. Zhu, Y. Luo, and Y. Li, "An inner current suppressing method for modular multilevel converters," *IEEE Trans. Power Electron.*, vol. 28, no. 11, pp. 4873–4879, Nov. 2013.

[8] M. Zhang, L. Huang, W. Yao, and Z. Lu, "Circulating harmonic current elimination of a CPS-PWM-Based modular multilevel converter with a plug-in repetitive controller," *IEEE Trans. Power Electron.*, vol. 29, no. 4, pp. 2083–2097, Apr. 2014.

[9] Q. Tu, Z. Xu, and L. Xu, "Reduced switching-frequency modulation and circulating current suppression for modular multilevel converters," *IEEE Trans. Power Del.*, vol. 26, no. 3, pp. 2009–2017, Jul. 2011.

[10] R. Picas, J. Pou, S. Ceballos, V. G. Agelidis, and M. Saeedifard, "Minimization of the capacitor voltage fluctuations of a modular multilevel converter by circulating current control," in *Proc. 38th Annu. Conf. IEEE Ind. Electron. Soc. (IECON)*, Oct. 2012, pp. 4985–4991.

[11] R. Picas, J. Pou, S. Ceballos, J. Zaragoza, G. Konstantinou, and V. G. Agelidis, "Optimal injection of harmonics in circulating currents of modular multilevel converters for capacitor voltage ripple minimization," in *Proc. IEEE ECCE Asia Downunder*, Melbourne, VIC, Australia, Jun. 2013, pp. 318–324.

[12] C. Xu, L. Lin, T. Yin, and J. Hu, "An improved phase-shifted-carrier technique for hybrid modular multilevel converter with boosted modulation index," *IEEE Trans. Power Electron.*, vol. 35, no. 2, pp. 1340–1352, Feb. 2020.

[13] A. J. Korn, M. Winkelnkemper, and P. Steimer, "Low output frequency operation of the modular multi-level converter," in *Proc. IEEE Energy Convers. Congr. Expo.*, Atlanta, GA, USA, Sep. 2010, pp. 3993–3997.

[14] J. Kolb, F. Kammerer, and M. Braun, "Straight forward vector control of the modular multilevel converter for feeding three-phase machines over their complete frequency range," in *Proc. 37th Annu. Conf. IEEE Ind. Electron. Soc. (IECON)*, Melbourne, VIC, Australia, Nov. 2011, pp. 1596–1601.

[15] J. Pou, S. Ceballos, G. Konstantinou, V. G. Agelidis, R. Picas, and J. Zaragoza, "Circulating current injection methods based on instantaneous information for the modular multilevel converter," *IEEE Trans. Ind. Electron.*, vol. 62, no. 2, pp. 777–788, Feb. 2015.

[16] A. Dekka, B. Wu, V. Yaramasu, and N. R. Zargari, "Model predictive control with common-mode voltage injection for modular multilevel converter," *IEEE Trans. Power Electron.*, vol. 32, no. 3, pp. 1767–1778, Mar. 2017.

[17] C. Zhao, Y. Li, G. Konstantinou, Z. Li, P. Wang, M. Lei, F. Xu, and Z. Liu, "Energy storage requirements of full-bridge modular multilevel converter with zero sequence voltage injection," in *Proc. 43rd Annu. Conf. IEEE Ind. Electron. Soc. (IECON)*, Beijing, China, Oct. 2017, pp. 4512–4517.

[18] R. Li, B. W. Williams, and J. E. Fletcher, "Influence of third harmonic injection on modular multilevel converter -based high-voltage direct current transmission systems," *IET Gener., Transmiss. Distrib.*, vol. 10, no. 11, pp. 2764–2770, Aug. 2016.
[19] G. Guo, Q. Song, W. Yang, Y. Wang, W. Liu, H. Rao, and S. Xu, "Application of third-order harmonic voltage injection in a modular multilevel converter," *IEEE Trans. Ind. Electron.*, vol. 65, no. 7, pp. 5260–5271, Jul. 2018.
[20] M. Vasiladiotis, N. Cherix, and A. Rufer, "Accurate voltage ripple estimation and decoupled current control for modular multilevel converters," in *Proc. 15th Int. Power Electron. Motion Control Conf. (EPE/PEMC)*, Sep. 2012, p. LS1a-1.
[21] C. Townsend, G. C. Goodwin, G. Konstantinou, N. Petranovic, G. Mirzaeva, G. Farivar, and J. Pou, "Identifying circulating currents and zero-sequence voltages for reduction in stored capacitor energy in modular multilevel converters," *IEEE Trans. Ind. Electron.*, Jan. 17, 2020, doi: 10.1109/TIE.2020.2965504.
[22] P. Dong, J. Lyu, and X. Cai, "Optimized design and control for hybrid MMC with reduced capacitance requirements," *IEEE Access*, vol. 6, pp. 51069–51083, 2018.
[23] A. Li, L. Lin, C. Xu, and S. Yang, "Coordinated optimization of capacitor voltage ripple and current stress minimization for modular multilevel converter," in *Proc. IEEE Int. Power Electron. Appl. Conf. Expo. (PEAC)*, Shenzhen, China, Nov. 2018, pp. 1–6.
[24] X. Li, Q. Song, W. Liu, S. Xu, Z. Zhu, and X. Li, "Performance analysis and optimization of circulating current control for modular multilevel converter," *IEEE Trans. Ind. Electron.*, vol. 63, no. 2, pp. 716–727, Feb. 2016.
[25] R. Słowinski, "Multiobjective network scheduling with efficient use of renewable and nonrenewable resources," *Eur. J. Oper. Res.*, vol. 7, no. 3, pp. 265–273, Jul. 1981.
[26] Y. Haimes, "Integrated system identification and optimization," *Control Dyn. Syst.*, vol. 10, pp. 435–518, 1973.
[27] A. Osyczka, *Multi-Criterion Optimization in Engineering With FORTRAN Programs*. New York, USA: Wiley, 1984.
[28] C. H. Tseng and T. W. Lu, "Minimax multiobjective optimization in structural design," *Int. J. Numer. Methods Eng.*, vol. 30, no. 6, pp. 1213–1228, Oct. 1990.
[29] E. Zitzler, K. Deb, and L. Thiele, "Comparison of multiobjective evolutionary algorithms: Empirical results," *Evol. Comput.*, vol. 8, no. 2, pp. 173–195, Feb. 2000.
[30] S. Rohner, S. Bernet, M. Hiller, and R. Sommer, "Modulation, losses, and semiconductor requirements of modular multilevel converters," *IEEE Trans. Ind. Electron.*, vol. 57, no. 8, pp. 2633–2642, Aug. 2010.
[31] Q. Song, W. Liu, X. Li, H. Rao, S. Xu, and L. Li, "A steady-state analysis method for a modular multilevel converter," *IEEE Trans. Power Electron.*, vol. 28, no. 8, pp. 3702–3713, Aug. 2013.
[32] E. Zitzler and L. Thiele, "Multiobjective optimization using evolutionary algorithms—A comparative case study," in *Parallel Problem Solving from Nature-PPSN V*. Berlin, Germany: Springer, 1998, pp. 292–301.
[33] K. Deb, A. Pratap, S. Agarwal, and T. Meyarivan, "A fast and elitist multiobjective genetic algorithm: NSGA-II," *IEEE Trans. Evol. Comput.*, vol. 6, no. 2, pp. 182–197, Apr. 2002.
[34] R. Zeng, L. Xu, L. Yao, and B. W. Williams, "Design and operation of a hybrid modular multilevel converter," *IEEE Trans. Power Electron.*, vol. 30, no. 3, pp. 1137–1146, Mar. 2015.
[35] W. Lin, D. Jovcic, S. Nguefeu, and H. Saad, "Full-bridge MMC converter optimal design to HVDC operational requirements," *IEEE Trans. Power Del.*, vol. 31, no. 3, pp. 1342–1350, Jun. 2016.
[36] L. Lin, Y. Lin, C. Xu, and Y. Chen, "Comprehensive analysis of capacitor voltage fluctuation and capacitance design for submodules in hybrid modular multilevel converter with boosted modulation index," *IEEE J. Emerg. Sel. Topics Power Electron.*, vol. 7, no. 4, pp. 2369–2383, Dec. 2019.

LEI LIN (Member, IEEE) was born in Jiangxi, China, in 1980. He received the B.S., M.S., and Ph.D. degrees in electrical engineering from the School of Electrical and Electronics Engineering (SEEE), Huazhong University of Science and Technology (HUST), Wuhan, China, in 2001, 2004, and 2007, respectively.

Since 2007, he has been involved in the teaching and research in the field of power electronics at SEEE, HUST. From 2007 to 2009, he was a Postdoctoral Fellow. From 2009 to 2010, he was a Lecturer. In 2010 and 2017, he was promoted to an Associate Professor and a Professor at the State Key Laboratory of Advanced Electromagnetic Engineering and Technology, SEEE, HUST, respectively. He has authored or coauthored more than 50 technical articles and holds over ten issued/pending patents. His current research interests include MMC for HVDC applications, high-voltage capacitor charging power supply, multilevel converters, and related control techniques.

Dr. Lin is the Associate Director of the Youth Working Committee of the China Power Supply Society. He is an Active Expert of the IEEE UPFC P2745 series.

ANG LI was born in Zhejiang, China, in 1994. He received the B.S. degree in electrical engineering from the School of Electrical and Electronics Engineering (SEEE), Huazhong University of Science and Technology (HUST), Wuhan, China, in 2016, where he is currently pursuing the M.S. degree in electrical and electronic engineering with the State Key Laboratory of Advanced Electromagnetic Engineering and Technology.

His research interest is high power converters for HVDC systems.

CHEN XU (Member, IEEE) was born in Hubei, China, in 1988. He received the B.S. and Ph.D. degrees in electrical engineering from the School of Electrical and Electronic Engineering (SEEE), Huazhong University of Science and Technology (HUST), Wuhan, China, in 2010 and 2016, respectively.

He is currently a Postdoctoral Fellow and a Research Assistant with the State Key Laboratory of Advanced Electromagnetic Engineering and Technology, SEEE, HUST. His research interests include flexible ac and dc transmission and distribution technology, power quality control, and multilevel converter.

YIFAN WANG was born in Huanggang, Hubei, China, in 1997. He received the B.S. degree in electrical engineering from the School of Electrical and Electronics Engineering (SEEE), Huazhong University of Science and Technology (HUST), Wuhan, China, in 2018, where he is currently pursuing the M.S. degree in electrical and electronic engineering with the State Key Laboratory of Advanced Electromagnetic Engineering and Technology.

His current research interest includes modeling, control, and stability analysis of power systems with high-voltage dc transmission.